Eur. Phys. J. B **44**, 491–500 (2005)
DOI: 10.1140/epjb/e2005-00149-8

THE EUROPEAN PHYSICAL JOURNAL B

Magnetization reversal in exchange biased Co/CoO patterns

E. Popova[1,2,a], H. Loosvelt[1], M. Gierlings[3], L.H.A. Leunissen[4], R. Jonckheere[4], C. Van Haesendonck[1], and K. Temst[1]

[1] Laboratorium voor Vaste-Stoffysica en Magnetisme, K.U. Leuven, Celestijnenlaan 200D, 3001 Leuven, Belgium
[2] Institute of Magnetism NASU, Vernadsky Blvd 36, 03142 Kyiv, Ukraine
[3] Hahn-Meitner-Institut, Glienicker Strasse 100, 14109 Berlin, Germany
[4] IMEC vzw, Kapeldreef 75, 3001 Leuven, Belgium

Received 6 October 2004
Published online 30 May 2005 –

Abstract. The influence of patterning on exchange bias has been investigated using arrays of micron-sized Co/CoO dots with different lateral confinement and length-to-width ratio. The patterned samples show higher coercive and exchange bias fields than a continuous Co/CoO bilayer. As in unpatterned film, magnetization reversal mechanisms on opposite sides of the hysteresis loops of the microstructured samples are different. However, with the increase of lateral confinement and shape anisotropy of the dots, the asymmetry in the magnetization reversal starts to differ from that observed in continuous Co/CoO films.

PACS. 75.60.Jk Magnetization reversal mechanisms – 61.12.Ha Neutron reflectometry

1 Introduction

Hysteresis loops exhibiting a characteristic shift away from the zero field axis initially have been observed in 1956 by Meiklejohn and Bean [1] for ferromagnetic Co particles having antiferromagnetic coating. This shift of the center of the hysteresis loop, referred to as exchange bias (EB) effect, is caused by a unidirectional magnetic anisotropy. It appears in thin film systems where an antiferromagnet (AF) is in contact with a ferromagnet (FM). The EB effect can be induced by cooling the AF/FM system from a temperature above the Curie temperature T_{Curie} to temperatures below the Néel temperature $T_{Néel}$ or below a certain blocking temperature T_B in an applied magnetic field. The blocking temperature can be equal to the Néel temperature or lower. If $T_{Néel}$ of the AF is higher than 300 K, the exchange bias can be created by bilayer deposition in a magnetic field. EB has been observed and studied in detail in a large variety of AF/FM systems (for reviews of most important experimental results and theoretical models, see Refs. [2–5]; the most up-to-date approach (domain state model for exchange bias) is developed in Ref. [6]). Despite the various experimental and theoretical studies on the subject, the microscopic origin of this effect is still not completely elucidated.

Recently, particular attention has been paid to the mechanisms of the magnetization reversal along a hysteresis loop, as the peculiarities of the reversal can provide crucial information about the processes taking place at the AF/FM interface on the microscopic level. Magnetization reversal in exchange biased continuous bilayers (Co/CoO [7–9], IrMn/NiFeCo and NiFe/NiMn [10], NiFe/MnNi [11], Fe/MnF_2 [12,13], Fe/FeF_2 [13], CoFe/IrMn [14], NiO/NiFe [15]) was studied by different techniques, for example, polarized neutron reflectometry [7–9,13], magnetometry [10,11], anisotropic magnetoresistance [12], high-resolution Kerr microscopy [14], magneto-optical indicator films [15], etc. Both mechanisms of magnetization reversal, rotation (coherent or incoherent) and domain nucleation and growth, were observed in exchange biased continuous films. The asymmetry of the reversal manifests itself either by different reversal mechanisms in the descending and ascending branches of a hysteresis loop [7–9,11–14] or by changes in the reversal mechanism as a function of the angle between the unidirectional anisotropy (defined by the cooling field direction) and the applied magnetic field direction during the measurement [14–17]. Moreover, the magnetization reversal depends on temperature [18,19] and on the distribution of the easy and hard axes of AF and FM and their orientation with respect to the unidirectional anisotropy axis and the applied magnetic field.

There exist only a few theoretical approaches explaining the observed reversal asymmetry. Within the framework of the domain state model, Beckmann et al. [20]

[a] *Present address*: LMOV-UVSQ, 45 av. des États-Unis, 78035 Versailles, France
e-mail: popova@physique.uvsq.fr

pointed out that the asymmetry of the magnetization reversal depends on the angle between the easy axis of the antiferromagnet and the applied magnetic field. A systematic variation of this angle reveals a rich variety of different reversal processes.

In the more specific case of a continuous Co/CoO bilayer or multilayer, at $T > T_{Néel}$ the reversal is symmetric along both descending and ascending branches of the hysteresis loop and occurs via rotation [9]. At $T < T_B$ the reversal takes place via domain nucleation in the descending branch of the initial hysteresis loop, and by rotation in the ascending branch of the same loop [7–9,18]. There exists evidence of symmetric reversal dominated by rotation along both branches of the so-called training loop, i.e., a hysteresis loop recorded subsequently to the initial loop without warming up the sample [21]. Furthermore, the asymmetry of the magnetization reversal is drastically reduced when the CoO thickness is increased [22].

Radu et al. [8] provide the following explanation of the reversal asymmetry. Along the descending hysteresis loop branch the magnetization reverses via domain nucleation and domain wall motion and leaves the Co/CoO interface in a magnetic multi-domain state. Due to the strong coupling of the interfacial spins to the antiferromagnet, they are not aligned along the applied field direction, even in saturation. When the applied field is increased from negative saturation, a torque is acting on the interfacial FM spins trying to reverse them back to the cooling field direction well before the magnetization reversal actually takes place. It seems that these interfacial FM domains are the seeds for the subsequent magnetization reversal by rotation along the ascending hysteresis branch and the branches of all following training loops. The break-up of the FM into domains during the initial magnetization reversal is supported by polarized neutron reflectometry (PNR) experiments [21] and magneto-optical imaging of a naturally oxidized Co film [23]. The AF state, locked-in after field cooling, is destroyed during the first magnetization reversal and domains are formed in the CoO layer. These domains pin the local magnetization of the coupled Co layer. The typical FM domain size measured for the initial reversal of a naturally oxidized Co layer with weak growth-induced anisotropy is about 5–10 μm [23].

In spite of the fact that there is no exhaustive description of the exchange bias effect at the microscopic level, the practical use of EB in microelectronics (spin valves, magnetic sensors or domain stabilizers in recording heads etc.) is already widespread. Miniaturization of electronics implies a constant decrease of the lateral size of the components. As the dimensions of the elements become comparable to the relevant magnetic length scales (spin diffusion length, domain size, domain wall width, etc.) the properties of such patterned structures deviate significantly from those of continuous films and therefore need to be investigated in detail [24–26].

Most of the experimental results and theoretical calculations point out that patterning affects the exchange bias [17,27–37]. However, there is no universal dependence of the exchange bias field on the lateral confinement. The EB field was reported to increase [29,31,34,37], to decrease [30,32,36] or to remain almost constant [35] with the reduction of dot size. It is difficult to infer systematic trends in the reported data because different materials (different anisotropies and AF and FM domain sizes), different dot spacing (different strength of dipolar interaction between the dots) and different structure forms (various shape anisotropy) were used.

The complexity of the exchange bias effect is conditioned, among other factors, by its dependence on magnetic and structural order of an antiferromagnet. Patterning affects the magnetic domain structure of AF: in patterned structures AF domain size becomes comparable to dot size thus removing the influence of the averaging of the AF domains on exchange bias. Even if a dot is large enough to accommodate a few magnetic domains, the domain walls will be strongly confined and the whole structure will behave differently from continuous film. The contribution of the dot edges into the domain configuration is also important since the edges could act as pinning center and stabilize AF domains. Also, the influence of the crystalline structure of AF on exchange coupling is more pronounced in small-sized patterns than in continuous films. For example, for a single domain single crystalline AF the layer at the interface with FM could be completely compensated or uncompensated. Therefore, the coupling between AF and FM will be strongly influenced by lateral confinement of the antiferromagnetic layer.

The general aim of our research is to understand the changes of the properties of exchange-biased films due to the patterning. On the one hand, we are interested in probing the influence of confinement and shape anisotropy on the exchange anisotropy and on the magnetization reversal. We are able to tailor the lateral dimensions of the dots in such a way that their size is comparable to the typical domain size in the ferromagnet [23] and the antiferromagnet. This is expected to yield new insights into the physical mechanisms governing exchange bias [37]. On the other hand, from the technological point of view it is important to be able to control exchange bias in patterned films in order to obtain a tunable source of anisotropy to stabilize the magnetization. This may enable to reduce the length scale that determines the superparamagnetic limit in magnetic recording ([29,38]).

The problem, which arises when dealing with patterned films, is the weak magnetic signal. Very few techniques are suitable for measuring this kind of samples. One of them is polarized neutron reflectometry [39,40], which is basically a vector magnetometry technique since it probes the magnetization components parallel and perpendicular to the applied field. Therefore, PNR offers the possibility to investigate the magnetization reversal mechanism in AF/FM bilayers. Off-specular PNR has been successfully used in studying arrays of patterned magnetic structures [41–44]. Off-specular reflectivity is characterized by resonant intensity peaks resulting from the in-plane periodicity of the patterned array. That way, even samples with low magnetic material coverage (few percents) can be investigated.

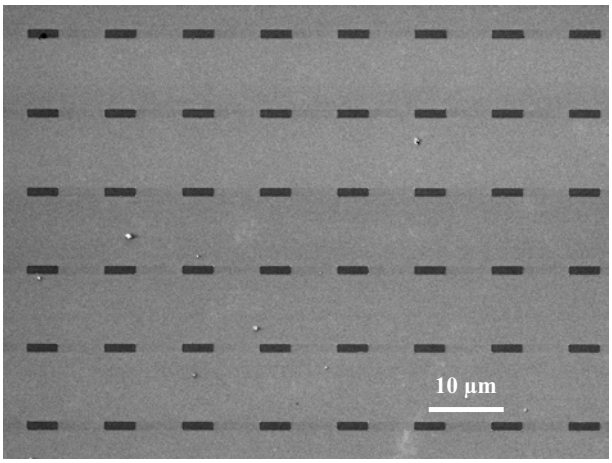

Fig. 1. Scanning electron microscope image of the sample with 1×4 μm^2 rectangles arranged within 10 μm period. Scan size is 80×60 μm^2.

2 Sample preparation and characterization

The samples were prepared by dc magnetron sputtering on an oxidized Si(111) wafer with SiO_2 thickness of 100 nm. The standard electron beam lithography procedure was used to pattern the wafer into dots of different size and shape. The cobalt layer deposition was performed simultaneously on a patterned and on a bare Si(111)/SiO_2 substrate. The latter piece was used as a reference film in characterization measurements. The growth of the 13 nm thick polycrystalline Co film was carried out at an Ar pressure of 3×10^{-3} Torr. After deposition the Co layer was exposed in-situ to pure O_2 gas for 90 s at a pressure of 1×10^{-4} Torr. A lift-off step removed the parts of the Co film on top of the resist, leaving a 2×2 cm^2 array of well-defined Co/CoO dots.

Two types of dots with different shape anisotropy were investigated: squares and rectangles. Two samples with square dots of 5×5 μm^2 and 3×3 μm^2 had the same periodicity of 15 μm. The squares covered 11% and 4% of the substrate respectively. The rectangles had dimensions of 1×4 μm^2 and were arranged within 10 μm period, covering 4% of the substrate. Figure 1 shows scanning electron microscopy image of the latter sample.

Thickness measurements were carried out on the continuous reference films using X-ray reflectivity. Table 1 summarizes the results for the three different patterns. Correlated roughness of the two interfaces (Co/CoO and CoO/air) provided the best fit to the experimental data. Correlated roughness of both interfaces in Co/CoO films was also observed using transmission electron microscopy by Gierlings [45].

Magnetization measurements were performed with a Superconducting Quantum Interference Device (SQUID) and with a Vibrating Sample Magnetometer (VSM) on patterned as well as on continuous reference samples. The reference samples exhibited an exchange bias shift after cooling from 300 K to 10 K in an applied field $H_{cool} = 0.4$ T. An abrupt magnetization reversal was observed in the descending hysteresis branch and a smooth reversal in the ascending branch, very similar to the results of Radu et al. [8] and Gierlings et al. [9] for continuous Co/CoO films and multilayers. The small CoO thickness led to a significant training effect as described in [22].

Table 1. Thickness of Co, CoO and correlated roughness of the references for the three investigated patterned samples.

Dots	t_{Co}, nm	t_{CoO}, nm	Roughness, nm
5×5 μm^2	11.8	1.5	0.7
3×3 μm^2	11.0	1.4	0.5
1×4 μm^2	11.5	1.5	0.6

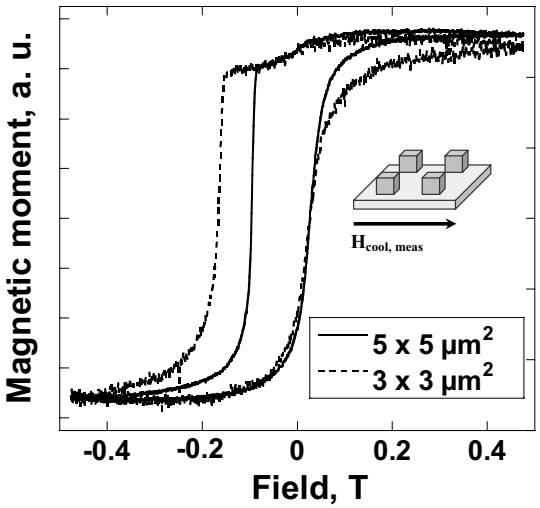

Fig. 2. VSM hysteresis loops for the samples with 5×5 μm^2 and 3×3 μm^2 squares within 15 μm period. The curves are recorded at 10 K after cooling in a field of 0.4 T along the edges of the squares. The directions of cooling and measurement field were the same.

Similarly to the continuous film, no exchange bias is observed in the patterned structures at 300 K. The coercive fields of the dot samples at 300 K are higher than those of the corresponding reference films. Shifted hysteresis loops are observed at 10 K after cooling the patterned samples in an applied field of 0.4 T (see Fig. 2 and Fig. 3b). Magnetization measurements at 300 K reveal a significant shape anisotropy of the sample patterned into rectangles (Fig. 3a). The easy magnetization axis is parallel to the long edge of the rectangles, while the hard axis is aligned along the short edge of the rectangles. Table 2 presents the values of the exchange bias and coercive fields for the investigated samples. Although the coercive field of the sample patterned into rectangles is different for the two field directions, the magnitude of exchange bias field is almost the same. This phenomenon was also observed for wire patterns [7,17] and explained in the framework of a coherent rotation model [17].

Similar to the unpatterned reference film, the hysteresis loops are asymmetric for the samples with dots: the magnetization reverses abruptly along the descending branch and smoothly along the ascending branch. However, in contrast to the continuous film, a pronounced kink

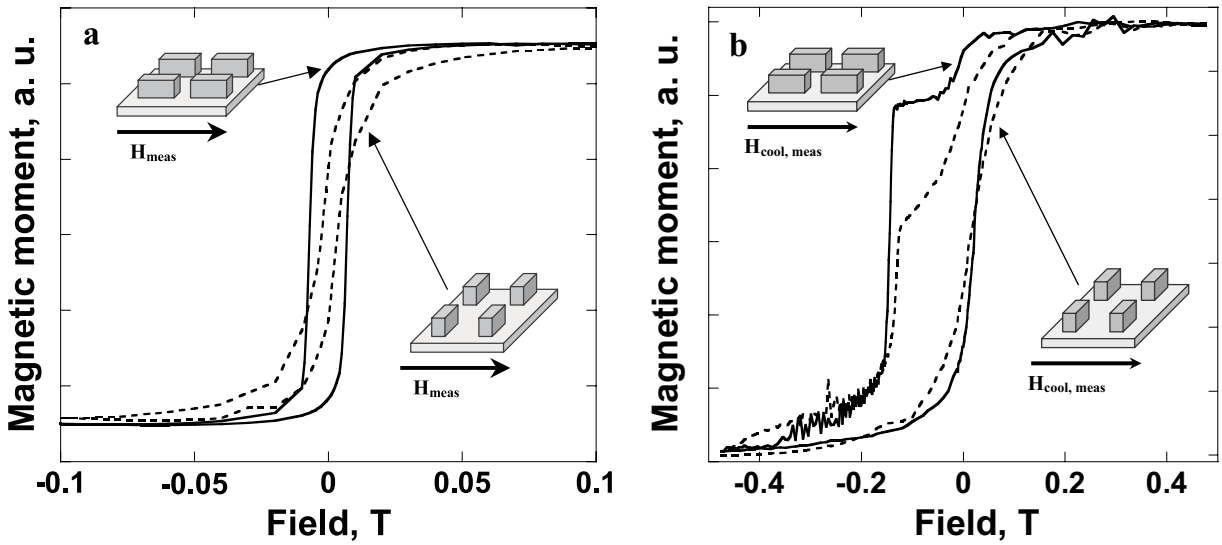

Fig. 3. (a) SQUID hysteresis loops of the sample with 1×4 μm^2 rectangles within 10 μm period. Measurements were performed at 300 K along long and short edge of the rectangles. (b) SQUID hysteresis loops of the sample with 1×4 μm^2 rectangles within 10 μm period. Measurements were performed at 10 K after cooling in a field of 0.4 T along long and short edge of the rectangles. The directions of cooling and measurement field were the same.

Table 2. Exchange bias and coercivity of the three investigated patterned samples measured at 10 K after cooling in a field of 0.4 T.

Dots	H_{meas} direction	H_C, T	H_{EB}, T
5×5 µm^2	→	0.0620	0.0355
3×3 µm^2	→	0.0965	0.0715
1×4 µm^2	→	0.0835	0.0625
1×4 µm^2	↗	0.0685	0.0615

is observed for all patterned films (Figs. 2 and 3b) along the descending branch between positive remanence and first coercive field. Such a kink was not observed for the reference samples.

Subsequently to the initial hysteresis loop recorded after the field cooling procedure, a second loop is measured. It exhibits the training effect (Fig. 4). The hysteresis curve is 'S'-shaped and symmetric; there is almost no kink in the trained loop.

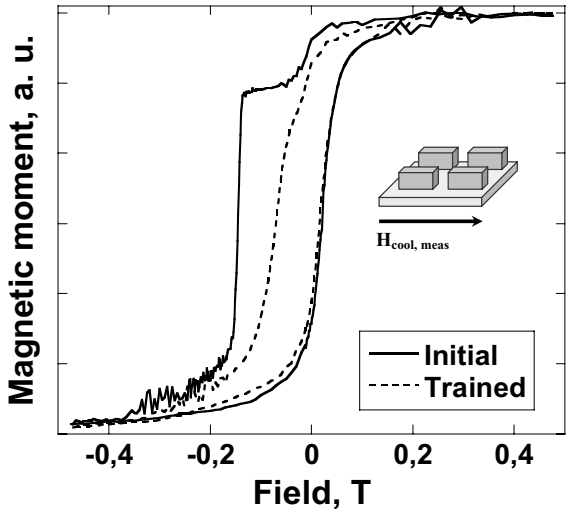

Fig. 4. SQUID hysteresis loops of the sample with 1×4 μm^2 rectangles within 10 μm period. The initial loop is measured at 10 K after field cooling in 0.4 T. Following the initial hysteresis curve, a trained loop is recorded at the same temperature.

3 Magnetization reversal

3.1 Experimental setup for off-specular neutron reflectometry measurements

Polarized neutron reflectometry measurements were performed using the V6 reflectometer at Hahn-Meitner Institut, Berlin. The description of the standard experimental setup can be found in reference [46]. A monochromatic neutron beam was used with a neutron wavelength of $\lambda = 0.466$ nm. A closed-cycle cryostat enabled to cool the samples down to 10 K. The small discrepancies between coercive fields measured by magnetometry and PNR are due to a non-perfect thermal contact between the sample and the sample holder in the PNR experiment. For the off-specular measurements the ^{3}He counters [46] were replaced by a position-sensitive detector (multiwire proportional counter) with an active area of about 180×180 mm^2 and a spatial resolution of 1.5 mm.

A simplified scheme of the neutron reflectivity experiment is presented in Figure 5. The incoming neutron beam hits the sample at an angle Θ_i and is reflected at an

angle Θ_f. Specular reflection occurs for $\Theta_i = \Theta_f$. Due to magnetic or structural roughness, neutrons will be reflected at $\Theta_i \neq \Theta_f$ and contribute to the off-specular signal. In case of periodic patterns, well-defined off-specular satellites are usually visible on both sides of the specular reflection peak. The positions of these satellites correspond to the lateral periodicity of the structures.

Using a polarized neutron beam, four neutron cross-sections I^{uu}, I^{dd}, I^{ud}, I^{du} were recorded. Here I denotes the intensity of the scattered neutron beam and the indices correspond to the neutron spin state before (first index) and after (second index) interaction with a sample. I^{uu} and I^{dd} are non-spin-flip (NSF) intensities, i.e. represent the interaction with a sample without change of the neutron spin direction. Spin-flip (SF) intensities I^{ud} and I^{du} are of purely magnetic origin and yield information about magnetization direction and reversal mechanism in magnetic films and structures.

As the amount of the magnetic material in the patterned samples was extremely small, the specular reflection supplied information mainly about the non-magnetic substrate. Therefore, an off-specular configuration has been used for the measurements. Magnetic information from a sample can be obtained measuring the off-specular intensity as a function of applied field. The magnetization reversal mechanism can be analyzed by separating the spin-flip and non-spin-flip contributions to the off-specular signal.

First of all, the angular range where the off-specular peak is visible has been determined carrying out a series of $\Theta - 2\Theta$ scans at magnetic saturation. The outcome of these scans is presented in a reciprocal space map for the rectangular pattern (Fig. 6). The specular ridge where $\Theta_i = \Theta_f$ is shown at $Q_x = 0$. Parallel to the specular ridge off-specular peak is clearly visible. The detector was then adjusted to the maximum intensity of the off-specular reflection and a field sweep has been performed covering the range from –0.48 T to 0.48 T. Spin analysis of the neutrons detected by a position-sensitive detector has been carried out.

Special cooling procedure was applied to avoid neutron depolarization during the measurements, since an external field of at least a few Gauss has to be applied to the sample in the direction parallel to the quantization axis of the incoming neutrons. The positive (negative) part of the hysteresis loop was measured after positive (negative) field cooling. This way, measurements were carried out in positive applied field for both branches of a hysteresis loop.

The direction of the incident neutron beam was perpendicular to the applied field. All the presented neutron data were corrected for the polarizer, flipper and analyzer efficiencies.

3.2 Square patterns

Two samples were investigated: 5×5 μm^2 and 3×3 μm^2 Co/CoO square dots with a 15 μm period. The dot sizes were comparable (5×5 μm^2) or smaller (3×3 μm^2) than

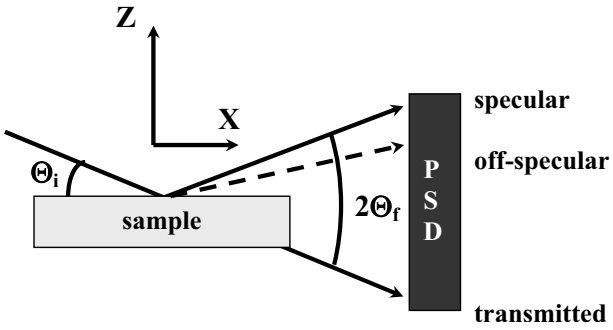

Fig. 5. Scattering geometry for specular and off-specular reflectivity measurements.

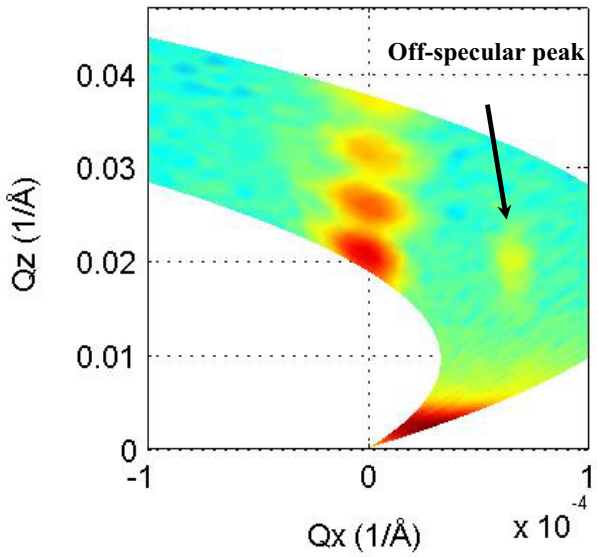

Fig. 6. Reciprocal space map recorded for the 1×4 μm^2 rectangular dots using spin-up neutrons. The sample was saturated in a field of 0.4 T. Uniform grey, light grey and dark grey colors correspond to the background signal, to the off-specular peak and to the reflected specular signal respectively.

the typical domain size reported for a Co/CoO bilayer [23]. This allowed us to study how the confinement imposed on the ferromagnet and antiferromagnet affects the exchange coupling between them.

In all experiments the external cooling and measurement magnetic fields were applied along one edge of the squares. The complete magnetic hysteresis loops of the samples with square dots were probed in the exchange bias state, i.e., after cooling of the samples in an applied field. Since the results obtained on both samples are qualitatively similar, the measurements performed on the 3×3 μm^2 patterns only will be presented in detail.

The sample was field cooled in –0.4 T along the edge of the squares and measured along the same edge. Figure 7a shows the PNR intensities measured along the descending hysteresis branch from positive remanence (0 T) through the first (negative) coercive field H_{C1} till negative saturation (–0.48 T). Because of the cooling in a negative field prior to the measurement, the NSF components I^{uu} and I^{dd} are inversed at positive remanence,

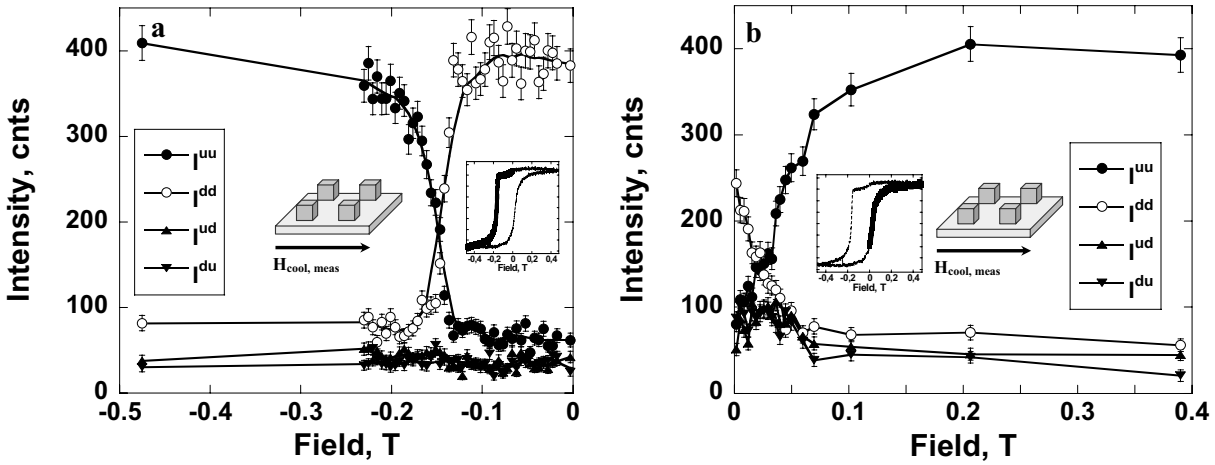

Fig. 7. (a) The four neutron cross-sections measured in off-specular configuration for fields along the descending hysteresis branch, i.e., from positive remanence through the first coercive field H_{C1} to negative saturation. The sample with 3×3 μm^2 squares was first cooled to 10 K in a field of –0.4 T. Cooling and applied fields were parallel to the edges of the squares. (b) The four neutron cross-sections measured in off-specular configuration for fields along the ascending hysteresis branch, i.e., from negative remanence through the second coercive field H_{C2} to positive saturation. The sample with 3×3 μm^2 squares was first cooled to 10 K in a field of 0.4 T. Cooling and applied fields were parallel to the edges of the squares.

i.e., $I^{uu} < I^{dd}$. As the negative field is increased, I^{uu} increases and I^{dd} decreases. They coincide at the coercive field $H_{C1} = -0.145$ T. When the sample reaches negative saturation at –0.48 T, I^{uu} becomes higher than I^{dd}, indicating that the magnetization has been reversed. It is obvious from Figure 7a that no increase of the SF signals I^{ud} and I^{du} above the background level is detected in the whole investigated field range. This implies that there is no magnetization component perpendicular to the applied external field. Therefore, it can be concluded that the reversal along the descending field branch occurs via domain nucleation and domain wall motion.

In order to measure the positive part of the hysteresis loop, the sample was field cooled in a positive field of 0.4 T, then saturated in a field of –0.48 T and measured along the ascending hysteresis branch starting from the negative remanence up to positive saturation (Fig. 7b). At negative remanence $I^{uu} < I^{dd}$ since the sample was previously saturated in negative fields. Around the second coercive field $H_{C2} = 0.025$ T both non-spin-flip components are equal while at positive saturation $I^{uu} > I^{dd}$. The spin-flip intensities are clearly enhanced close to coercive field. The relative increase in comparison with the spin-flip intensities at saturation is 2.9 ($\pm$ 0.5) times. For the same measurement performed on 5×5 μm^2 square patterns the ratio $I^{SF}(H_{C2})/I^{SF}(H_{sat})$ is about 7.0 ($\pm$ 1.0). However, even for 5×5 μm^2 squares I^{SF} at the second coercive field doesn't overcome the non-spin-flip intensity value, contrary to the results reported for continuous Co/CoO films [7,8]. Obviously, only a part of the magnetization of patterned samples reverses by rotation along the ascending hysteresis branch. This rotating part of the magnetization is larger in larger structures, i.e., the higher is the lateral confinement, the smaller part of the magnetization reverses via rotation process at second coercive field.

One of the goals of our experiments was to study in detail the magnetization behavior in the field region between the first remanence and the first coercive field (on the descending branch). A kink in the magnetometry hysteresis loop was observed in this field range. In order to compare VSM and PNR data, PNR hysteresis loop has been calculated using spin asymmetry: $SA = (I^{uu} - I^{dd})/(I^{uu} + I^{dd} + I^{ud} + I^{du})$. In the kink region the increased noise in the non-spin-flip intensities was observed by PNR (Fig. 8).

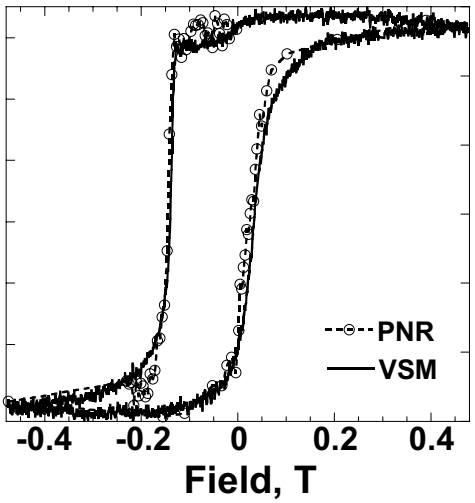

Fig. 8. Comparison between the PNR and VSM hysteresis loops measured for the sample with 3×3 μm^2 squares after cooling to 10 K in a field of 0.4 T. Cooling and applied fields were parallel to the edges of the squares.

3.3 Rectangular pattern

For the case of a rectangular pattern the length-to-width ratio was increased in comparison to the previously described square dots. The sample exhibited a pronounced shape anisotropy (Fig. 3a). During the PNR experiments,

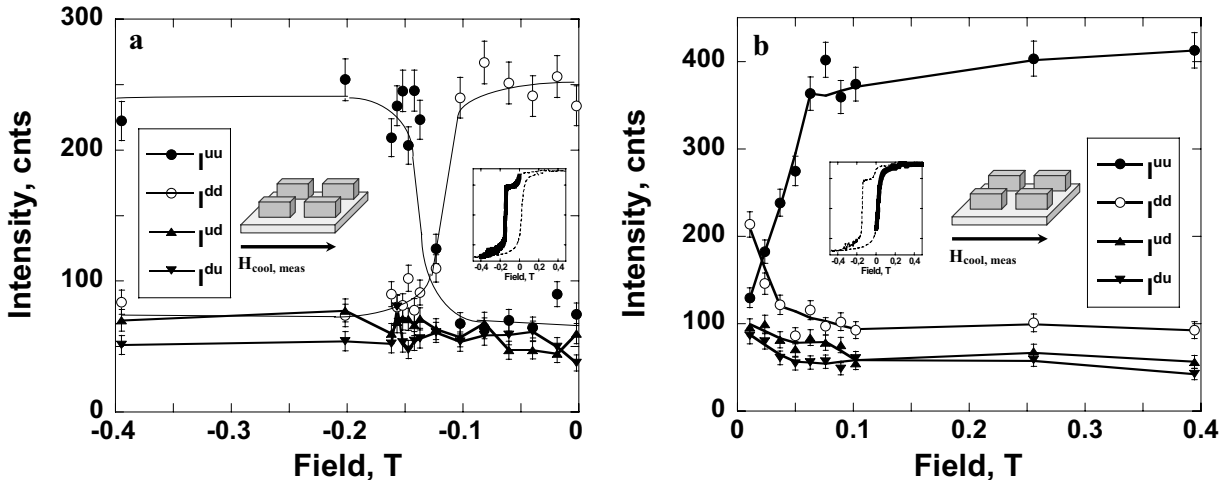

Fig. 9. (a) The four neutron cross-sections measured in off-specular configuration for fields along the descending hysteresis branch, i.e., from positive remanence through the first coercive field H_{C1} to negative saturation. The sample with 1×4 μm^2 rectangles was first cooled to 10 K in a field of –0.4 T. Cooling and applied fields were parallel to the long edges of the rectangles. (b) The four neutron cross-sections measured in off-specular configuration for fields along the ascending hysteresis branch, i.e., from negative remanence through the second coercive field H_{C2} to positive saturation. The sample with 1×4 μm^2 rectangles was first cooled to 10 K in a field of 0.4 T. Cooling and applied fields were parallel to the long edges of the rectangles.

the external magnetic field has been applied either along in-plane easy axis or along hard axis of the structures. Therefore, not only the influence of the confinement, but also of the shape anisotropy on the exchange bias was investigated.

In the PNR experiment I the complete magnetic hysteresis of the sample with rectangular dots has been probed along the easy magnetization axis. First, the sample was field cooled in –0.4 T along the long edge of the rectangles and then measured along the same edge. Figure 9 shows the outcome of the experiment. As in the case of square dots, the magnetization reversal is dominated by domain nucleation and domain wall motion in the descending hysteresis branch. However, a slight (≈10%) increase of the spin-flip signal is observed between first coercive field H_{C1} and negative saturation. The field region where both spin-flip intensities I^{ud} and I^{du} increase corresponds to the slow decrease of the magnetic moment in the SQUID hysteresis loop just after the sharp reversal at H_{C1} and before negative saturation (Fig. 3b). Hence, small part of the sample magnetization seems to reverse via rotation. The rotation is assumed to take place at the FM/AF interface and/or within the domains that appeared during the initial magnetization reversal.

Along the ascending hysteresis branch only a part of the magnetization is perpendicular to the neutron spin at H_{C2}. The ratio $I^{SF}(H_{C2})/I^{SF}(H_{sat}) = 1.83\,(\pm 0.07)$ is even lower than for the sample patterned in 3×3 μm^2 squares.

Similar reversal mechanisms are observed for the case when field cooling and measurement are applied along the short edge of the rectangles, i.e. along the hard axis of the patterned structure (experiment II, not shown). Here $I^{SF}(H_{C2})/I^{SF}(H_{sat}) = 1.35\,(\pm 0.03)$.

In the experiment III the sample was field cooled along the easy magnetization axis (long edge of the rectangles).

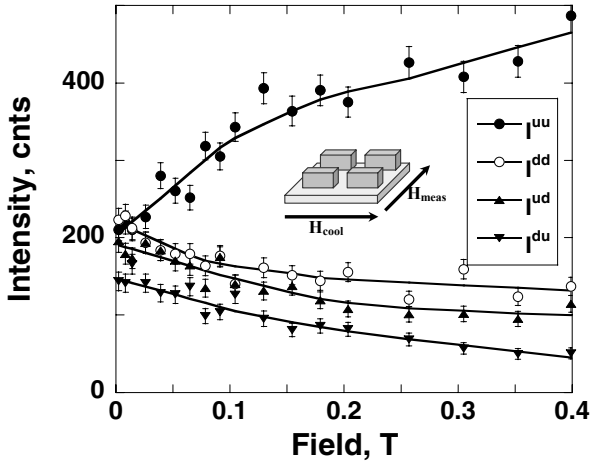

Fig. 10. The four neutron cross-sections measured in off-specular configuration for the case when cooling field was perpendicular to the measurement field. The cooling field of 0.4 T has been applied along the long edge of rectangles, then the sample has been turned by 90° and was measured at 10 K along the short edge of the rectangles in increasing field from 0 T to 0.4 T.

Then the applied field was decreased and the sample was rotated in zero field by 90°. The measurement was then performed along the hard axis (short edge of the rectangles) increasing the field from 0 T to 0.4 T (see Fig. 10). In this measurement configuration one does not expect to observe any exchange bias [17]. At the applied field of 0.002 T the non-spin-flip components are equal suggesting that there is no net magnetization component along the applied field. There are two possible arrangements of the sample magnetization that lead to this result: either the sample has broken into magnetic domains with the resulting zero net magnetization or the sample magnetization

is perpendicular to the neutron spin direction (and to applied measurement field in the present configuration). As the sample magnetization is still in the remanence state, the former possibility can be excluded. Moreover, at this field $I^{SF} \approx I^{NSF}$. The fact that the spin-flip signal is two times higher in this measurement configuration than at the second coercive field (in the measurement where the cooling and the measurement fields were collinear, experiment I, see Fig. 9b) confirms that for the latter only part of the sample magnetization was rotating at H_{C2}. As the applied field is increased, the spin-flip components decrease slowly, indicating that the magnetization is rotating away from the easy axis of the dots (defined by both the easy magnetization axis and the induced unidirectional anisotropy) towards the applied field direction. This rotation continues up to field of 0.4 T. It seems that even at 0.4 T the patterned film is not yet saturated.

When the field is set back to 0.002 T, the spin-flip intensities are almost as high as after the sample rotation (contrary to the results reported in [21], where a decrease of 50% was observed). However, the non-spin-flip components are no longer equal: $I^{uu} > I^{dd}$ (not shown in Fig. 10). Apparently, there is not only a large component of the sample magnetization perpendicular to the field direction but also a significant magnetization component parallel to the external field. After this measurement, the sample was subjected to –0.4 T, then the field was set to 0.002 T and the four cross-sections were measured again. In this case the relation $I^{uu} < I^{dd}$ still holds, with absolute values of I^{uu} and I^{dd} corresponding to the previous measurement. This implies that either a small part of the sample magnetization is following the applied field while the major part of the magnetization is aligned parallel to the easy axis or that the magnetization is tilted. In this experiment it was not possible to distinguish between the situation where the magnetization of the whole sample is tilted in the film plane with respect to the applied field direction (single domain state) and the situation where some parts of magnetization are orthogonal.

The experiment IV was dedicated to the investigation of the training effect in Co/CoO rectangles. For this purpose, the sample was field cooled to 10 K in a field of 0.4 T. Then the first hysteresis loop and two training loops were cycled under influence of the external magnetic field. The spin-flip signal was monitored near the first and second coercive fields. The magnetization reversal mechanism along the descending branches of two training hysteresis loops is different from that of the initial loop, i.e. part of the magnetization reverses by rotation along the descending branch of the training loop.

4 Discussion

The asymmetry of the magnetization reversal reported for continuous Co/CoO films is preserved in micron-sized dots with different shape anisotropy, i.e., the reversal mechanisms in the opposite hysteresis branches are still different. For the square structures, the reversal along the descending branch of the initial hysteresis loop occurs via domain nucleation and domain wall motion. In contrast, for the ascending branch, i.e., when the applied field is increased from $-H_{sat}$ to $+H_{sat}$, only a part of the magnetization rotates towards the positive saturation. The smaller are the elements of the patterns, the smaller part of the magnetization takes part in the rotation process. Therefore, the lateral confinement of the magnetic structure to the micrometer size indeed affects the magnetization reversal.

The influence of the size reduction is also clearly visible in the appearance of a kink on the descending branch of the hysteresis curve. This kink cannot be attributed to the dipolar coupling between the elements within the pattern only [28], since the interaction between dots in all studied patterns can be neglected for the used inter-dot distances [25]. The existence of this kink can be explained by the presence of a partly unbiased Co layer and is most probably related to the grain size and structure of polycrystalline Co/CoO films. Minor hysteresis loops recorded in the kink region are symmetrical around zero field axis and exhibit coercive fields comparable to those of unbiased Co film. Cycling the applied field along the minor loops does not affect the exchange bias in a sample. The resulting hysteresis loop (as in Fig. 2, 3b and 4) is the superposition of two loops corresponding to biased and unbiased part of the sample. A training effect is observed only if the field corresponding to the sharp edge of the initial hysteresis loop has been overcome. As soon as the strength of the applied magnetic field exceeds the strength of the EB pinning at the interface, the interfacial magnetic structure is irreversibly changed and the training effect appears in the subsequently recorded hysteresis loop.

The magnetization reversal asymmetry is also observed for the rectangular pattern, where the length-to-width ratio is more pronounced than for square dots. A single domain state and strong shape anisotropy of the 1×4 μm^2 Co dots at 300 K were confirmed by Temst et al. [43]. This result is valid for the Co/CoO rectangles of the same size as well. However, in contrast to the case of the square dots, the magnetization reversal along the descending hysteresis branch occurs via domain nucleation with subsequent rotation in the field region between first coercive field and negative saturation. The magnetization rotation can occur at the FM/AF interface or/and can take place within the magnetic domains that are created in a sample during the first magnetization reversal. As for the magnetization reversal in the ascending hysteresis branch, the comparison of the spin-flip signal in the experiments I and III (Figs. 9b and 10) confirms that, as in case of the square pattern, only part of the sample magnetization reverses by rotation. This rotating part is slightly higher for the configuration when cooling and measurement fields are applied along the long edge of the rectangles.

Apparently, lateral confinement of the Co/CoO bilayer to the micrometer size and pronounced shape anisotropy affect the magnetization reversal mechanism. As has been reported recently, for Co/CoO wires having a width-to-length ratio of 10 000 the magnetization reversal becomes

symmetric and occurs via domain nucleation and domain wall motion along both branches of the hysteresis curve for an applied field aligned parallel to the wires [7]. For the presently described rectangular pattern the length-to-width ratio is 4 and the onset of the magnetization reversal mechanism change can be observed.

We hope that our experiments will stimulate further development of the theoretical models describing exchange bias effect in patterned and continuous AF/FM layers.

5 Conclusions

The influence of patterning on the magnetization reversal in exchange biased structures was studied. Co/CoO bilayers were patterned into micrometer size dots of different shape.

The patterned samples show higher coercive and exchange bias fields than a continuous reference film at 10 K after field cooling procedure. Shape anisotropy doesn't affect the exchange bias strength, but modifies magnetization reversal and hysteresis loop shape.

For the patterns studied here the asymmetry of the magnetization reversal on opposite sides of the same hysteresis loop is preserved in spite of the lateral confinement: domain nucleation and domain wall motion dominates the reversal for the descending branch whereas rotation processes occur in the ascending branch. However, for micrometer size dots the magnetization reversal, being still asymmetric, starts to differ from the magnetization reversal observed for continuous films.

The authors are thankful to D. Buntinx for scanning electron microscope images, to M.J. Van Bael for SQUID loops on the sample patterned into rectangles, to J. Moonens for the assistance with the patterned wafer and to H. Fritzsche for fruitful discussions about PNR. This work was supported by the Fund for Scientific Research – Flanders (FWO), the Flemish GOA and Belgian IAP programs, QMDS Research and Training Network (HPRN-CT-2000-00134). The support by the European Community under the Access to Research Infrastructures Action of the Human Potential Program (HPRI-CT-2001-00138) and under the 6th Framework Program through the Key Action: Strengthening the European Research Area, Research Infrastructures (RII3-CT-2003-505925 (NMI3)) is acknowledged as well.

References

1. W.H. Meiklejohn, C.P. Bean, Phys. Rev. **102**, 1413 (1956)
2. J. Nogués, I.K. Schuller, J. Magn. Magn. Mater. **192**, 203 (1999)
3. A.E. Berkowitz, K. Takano, J. Magn. Magn. Mater. **200**, 552 (1999)
4. R.L. Stamps, J. Phys. D: Appl. Phys. **33**, R247 (2000)
5. M. Kiwi, J. Magn. Magn. Mater. **234**, 584 (2001)
6. U. Nowak, K.D. Usadel, J. Keller, P. Miltényi, B. Beschoten, G. Güntherodt, Phys. Rev. B **66,** 014430 (2002)
7. H. Loosvelt, E. Popova, J. Swerts, D. Buntinx, J. Bekaert, C. Van Haesendonck, H. Fritzsche, K. Temst (submitted to Solid State Commun.)
8. F. Radu, M. Etzkorn, R. Siebrecht, T. Schmitte, K. Westerholt, H. Zabel, Phys. Rev. B **67**, 134409 (2003)
9. M. Gierlings, M.J. Prandolini, H. Fritzsche, M. Gruyters, D. Riegel, Phys. Rev. B **65**, 092407 (2002)
10. T. Hughes, K. O'Grady, H. Laidler, R.W. Chantrell, J. Magn. Magn. Mater. **235**, 329 (2001)
11. D. Spenato, S.P. Pogossian, H. Le Gall, J. Magn. Magn. Mater. **262**, 294 (2003)
12. C. Leighton, M. Song, J. Nogués, M.C. Cyrille, I.K. Schuller, J. Appl. Phys. **88**, 344 (2000)
13. M.R. Fitzsimmons, P. Yashar, C. Leighton, I.K. Schuller, J. Nogués, C.F. Majkrzak, J.A. Dura, Phys. Rev. Lett. **84**, 3986 (2000)
14. J. McCord, R. Schäfer, R. Mattheis, K.-U. Barholz, J. Appl. Phys. **93**, 5491 (2003)
15. V.I. Nikitenko, V.S. Gornakov, L.M. Dedukh, Yu.P. Kabanov, A.F. Khapikov, A.J. Shapiro, R.D. Shull, A. Chaiken, R.P. Michel, Phys. Rev. B **57**, R8111 (1998)
16. A. Kirilyuk, Th. Rasing, H. Jaffrès, D. Lacour, F. Nguyen Van Dau, J. Appl. Phys. **91**, 7745 (2002)
17. A. Hoffmann, M. Grimsditch, J.E. Pearson, J. Nogués, W.A.A. Macedo, I.K. Schuller, Phys. Rev. B **67**, 220406(R) (2003)
18. W.-T. Lee, S.G.E. te Velthuis, G.P. Felcher, F. Klose, T. Gredig, E.D. Dahlberg, Phys. Rev. B **65**, 224417 (2002)
19. M.R. Fitzsimmons, C. Leighton, A. Hoffmann, P.C. Yashar, J. Nogués, K. Liu, C.F. Majkrzak, J.A. Dura, H. Fritzsche, I.K. Schuller, Phys. Rev. B **64**, 104415 (2001)
20. B. Beckmann, U. Nowak, K.D. Usadel, Phys. Rev. Lett. **91**, 187201 (2003)
21. S.G.E. te Velthuis, A. Berger, G.P. Felcher, B.K. Hill, E.D. Dahlberg, J. Appl. Phys. **87**, 5046 (2000)
22. T. Gredig, I.N. Krivorotov, E.D. Dahlberg, J. Appl. Phys. **91**, 7760 (2002)
23. U. Welp, S.G.E. te Velthuis, G.P. Felcher, T. Gredig, E.D. Dahlberg, J. Appl. Phys. **93**, 7726 (2003)
24. M.I. Montero, K. Liu, O.M. Stoll, A. Hoffmann, J.J. Åkerman, J.I. Martín, J.L. Vicent, S.M. Baker, T.P. Russell, C. Leighton, J. Nogués, I.K. Schuller, J. Phys. D: Appl. Phys. **35**, 2398 (2002)
25. J.I. Martín, J. Nogués, K. Liu, J.L. Vicent, I.K. Schuller, J. Magn. Magn. Mater. **256**, 449 (2003)
26. F. J. Himpsel, J.E. Ortega, G.J. Mankey, R.F. Willis, Adv. Phys. **47**, 511 (1998)
27. R.E. Dunin-Borkowski, M.R. McCartney, B. Kardynal, M.R. Scheinfein, D.J. Smith, S.S.P. Parkin, J. Appl. Phys. **90**, 2899 (2001)
28. E. Girgis, R.D. Portugal, H. Loosvelt, M.J. Van Bael, I. Gordon, M. Malfait, K. Temst, C. Van Haesendonck, L.H.A. Leunissen, R. Jonckheere, Phys. Rev. Lett. **91**, 187202 (2003)
29. K. Liu, S.M. Baker, M. Tuominen, T.P. Russell, I.K. Schuller, Phys. Rev. B **63**, 060403(R) (2001)
30. M. Fraune, U. Rüdiger, G. Güntherodt, S. Cardoso, P. Freitas, Appl. Phys. Lett. **77**, 3815 (2000)
31. Z.B. Guo, Y.K. Zheng, K.B. Li, Z.Y. Liu, P. Luo, Y.H. Wu, J. Appl. Phys. **95**, 4918 (2004)
32. J. Sort, B. Dieny, M. Fraune, C. Koenig, F. Lunnebach, B. Beschoten, G. Güntherodt, Appl. Phys. Lett. **84**, 3696 (2004)

33. T. Pokhil, D. Song, E. Linville, J. Appl. Phys. **91,** 6887 (2002)
34. L. Sun, Y. Ding, C.L. Chien, P.C. Searson, Phys. Rev. B **64**, 184430 (2001)
35. J. Yu, A.D. Kent, S.S.P. Parkin, J. Appl. Phys. **87**, 5049 (2000)
36. Y. Shen, Y. Wu, H. Xie, K. Li, J. Qiu, Z. Guo, J. Appl. Phys. **91**, 8001 (2002)
37. S. Zhang, Z. Li, Phys. Rev. B **65**, 054406 (2001)
38. V. Skumryev, S. Stoyanov, Y. Zhang, G. Hadjipanayis, D. Givord, J. Nogués, Nature **423**, 850 (2003)
39. S.J. Blundell, J.A.C. Bland, Phys. Rev. B **46**, 3391 (1992)
40. H. Zabel, K. Theis-Bröhl, J. Phys.: Condens. Matter **15**, S505 (2003)
41. K. Theis-Bröhl, T. Schmitte, V. Leiner, H. Zabel, K. Rott, H. Brückl, J. McCord, Phys. Rev. B **67,** 184415 (2003)
42. K. Temst, M.J. Van Bael, H. Fritzsche, Appl. Phys. Lett. **79**, 991 (2001)
43. K. Temst, M.J. Van Bael, V.V. Moshchalkov, Y. Bruynseraede, H. Fritzsche, R. Jonckheere, Appl. Phys. A **74** [Suppl.], S1538 (2002)
44. M.R. Fitzsimmons, S.D. Bader, J.A. Borchers, G.P. Felcher, J.K. Furdyna, A. Hoffmann, J.B. Kortright, I.K. Schuller, T.C. Schulthess, S.K. Sinha, M.F. Toney, D. Weller, S. Wolf, J. Magn. Magn. Mater. **271**, 103 (2004)
45. M. Gierlings, Ph.D. thesis, Freien Universität Berlin, 2002
46. F. Mezei, R. Golub, F. Klose, H. Toews, Physica B **213–214**, 898 (1995)